Inorganic Chemistry

Article

pubs.acs.org/IC

Osmium(III) Analogues of KP1019: Electrochemical and Chemical Synthesis, Spectroscopic Characterization, X-ray Crystallography, Hydrolytic Stability, and Antiproliferative Activity

Paul-Steffen Kuhn,[†] Gabriel E. Büchel,[†,‡] Katarina K. Jovanović,[§] Lana Filipović,[§] Siniša Radulović,[§] Peter Rapta,[⊥] and Vladimir B. Arion*[,†]

[†]Faculty of Chemistry, Institute of Inorganic Chemistry, University of Vienna, Währinger Strasse 42, A-1090 Vienna, Austria

[‡]Division for Physical Sciences & Engineering and KAUST Catalysis Center, King Abdullah University of Science and Technology, Thuwal, Saudi Arabia

[§]Institute for Oncology and Radiology of Serbia, Pasterova 14, 11000 Belgrade, Serbia

[⊥]Department of Physical Chemistry, Slovak University of Technology, Radlinského 9, SK-81237 Bratislava, Slovak Republic

Supporting Information

ABSTRACT: A one-electron reduction of osmium(IV) complexes *trans*-[$Os^{IV}Cl_4$(Hazole)$_2$], where Hazole = 1*H*-pyrazole ([**1**]^0), 2*H*-indazole ([**2**]^0), 1*H*-imidazole ([**3**]^0), and 1*H*-benzimidazole ([**4**]^0), afforded a series of eight new complexes as osmium analogues of KP1019, a lead anticancer drug in clinical trials, with the general formula (cation)[*trans*-$Os^{III}Cl_4$(Hazole)$_2$], where cation = H_2pz^+ (H_2pz[**1**]), H_2ind^+ (H_2ind[**2**]), H_2im^+ (H_2im[**3**]), Ph_4P^+ (Ph_4P[**3**]), nBu_4N^+ (nBu_4N[**3**]), H_2bzim^+ (H_2bzim[**4**]), Ph_4P^+ (Ph_4P[**4**]), and nBu_4N^+ (nBu_4N[**4**]). All complexes were characterized by elemental analysis, ^{1}H NMR spectroscopy, electrospray ionization mass spectrometry, UV−vis spectroscopy, cyclic voltammetry, while H_2pz[**1**], H_2ind[**2**], and nBu_4[**3**], in addition, by X-ray diffraction. The reduced species [**1**]$^-$ and [**4**]$^-$ are stable in aqueous media in the absence of air oxygen and do not react with small biomolecules such as amino acids and the nucleotide 5′-dGMP. Cell culture experiments in five different human cancer cell lines (HeLa, A549, FemX, MDA-MB-453, and LS-174) and one noncancerous cell line (MRC-5) were performed, and the results were discussed and compared to those for KP1019 and cisplatin. Benzannulation in complexes with similar structure enhances antitumor activity by several orders of magnitude, implicating different mechanisms of action of the tested compounds. In particular, complexes H_2ind[**2**] and H_2bzim[**4**] exhibited significant antiproliferative activity *in vitro* when compared to H_2pz[**1**] and H_2im[**3**].

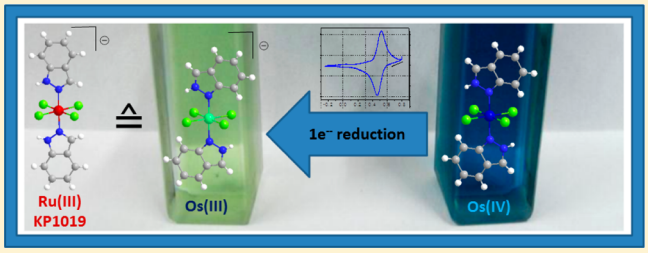

INTRODUCTION

Over the past decades the field of ruthenium- and osmium-based antitumor agents has attracted continuous interest.[1,2] The synthesis of new organometallic[3−8] and coordination compounds[9−12] as well as their spectroscopic properties and antiproliferative activity *in vitro* and *in vivo* have been reported. However, only two potential ruthenium anticancer agents are in clinical trials, namely, [$Ru^{III}Cl_4$(Hind)$_2$]$^-$ (NKP-1339/KP1019, Hind = 1*H*-indazole)[13,14] and (H_2im)[$Ru^{III}Cl_4$(DMSO)(Him)] (NAMI-A, Him = 1*H*-imidazole, DMSO = dimethyl sulfoxide)[15] (Chart 1). The first one is active against a variety of advanced and metastatic solid malignancies, most promising in nonsmall cell lung cancer and gastrointestinal neuroendocrine tumors,[16] whereas the second one mainly acts as an antimetastatic drug with a current research focus on lung cancer.[17]

Attempts to prepare related osmium complexes have also been undertaken, and these are well-documented in the literature.[18−20] While potential antitumor activity of osmium complexes was discovered in the 1970s,[21] the synthesis, spectroscopic, and first biological investigations of the osmium(IV) analogue of KP1019[18] as well as the Os-NAMI-A-type complexes[19] have been reported quite recently. [$Os^{IV}Cl_4$(Hazole)$_2$] showed comparable cytotoxicity to their

Chart 1. Ruthenium Complexes in Clinical Trials

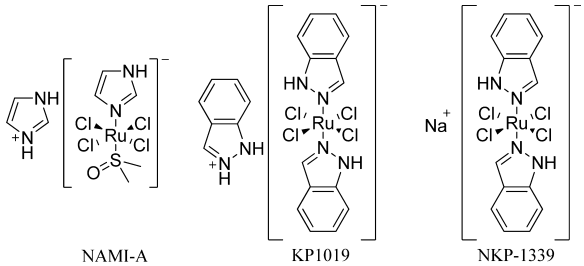

Received: July 17, 2014
Published: October 7, 2014

   dx.doi.org/10.1021/ic501710k | *Inorg. Chem.* 2014, 53, 11130−11139

ruthenium(III) congeners and a higher stability in aqueous solution. However, the solubility of these neutral complexes in 1% DMSO/water was borderline for the *in vitro* testing of their antiproliferative activity.[11,18] Furthermore, the first osmium(VI)−nitrido complexes with azole heterocycles have been found to possess potential antitumor properties.[9]

Although ruthenium and osmium belong to the same group of the periodic table, there are distinct differences between the two metals and their coordination chemistry, such as the ability of osmium to stabilize higher oxidation states, the magnitude of spin−orbit coupling, the rate of metal−ligand exchange reactions, and their behavior toward hydrolysis.[20,22]

Indazole is usually referred to as 1*H*-indazole, which is the predominant form in the gaseous phase and aqueous solution. Two other tautomers, 2*H*-indazole and 3*H*-indazole, are also well-documented (Chart 2).[23,24] There has been some evidence

Chart 2. Tautomeric Forms of Indazole

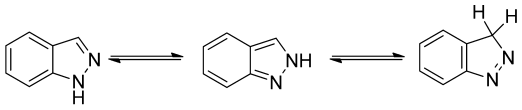

that the indazole tautomer identity has an impact on biological properties.[25−27] Recent investigations on the antiproliferative activity of $[Os^{IV}Cl_5(Hind)]^-$, where Hind is 1*H*- or 2*H*-indazole, showed different results *in vitro* and *in vivo*. The 2*H*-tautomer was found to be superior in the three human cancer cell lines CH1 (ovarian carcinoma), SW480 (colon carcinoma), and A549 (nonsmall cell lung cancer), but inferior in a Hep3B SCID mouse xenotransplantation model.[11]

These results encouraged us to further investigate the influence of the indazole tautomer identity on physicochemical and biological properties of their osmium complexes. The $[Os^{IV}Cl_4(Hazole)_2]$ compounds were regarded by us as suitable precursors for the synthesis of osmium(III) analogues of KP1019 by electrochemical and chemical reduction. These reduced species were expected to be more soluble in aqueous media than the parent osmium(IV) compounds. The aqueous solubility is an important property that has an impact on a drug's bioavailability and corroborates the antiproliferative activity assay data *in vitro*.[28] In addition, it was intriguing to find out whether the coordination mode of indazole remains intact upon one-electron reduction.

Herein we report the electrochemical and chemical synthesis, spectroscopic characterization, and X-ray diffraction studies of complexes of the general formula $(cation)[Os^{III}Cl_4(Hazole)_2]$, where cation = azolium, tetrabutylammonium, or tetraphenylphosphonium, while Hazole = 1*H*-pyrazole, 2*H*-indazole, 1*H*-imidazole, and 1*H*-benzimidazole (Chart 3). The antiproliferative activity of complexes H_2pz[**1**], H_2ind[**2**], H_2im[**3**], and H_2bzim[**4**] was tested in five different human cancer cell lines (HeLa, A549, FemX, MDA-MB-453, and LS-174) and one nontumorigenic cell line (MRC-5), and the obtained data were compared to those of KP1019 and cisplatin.

EXPERIMENTAL SECTION

Materials. Solvents were obtained from commercial sources and used as received. OsO_4 (99.8%) was purchased from Johnson Matthey, while 1*H*-pyrazole, 1*H*-indazole, 1*H*-imidazole, and 1*H*-benzimidazole as well as $NaBH_4$, nBu_4NBH_4, and nBu_4NCl from Sigma-Aldrich. All chemicals were used without further purification. The starting compounds $[Os^{IV}Cl_4(Hazole)_2]$ (Hazole = 1*H*-pyrazole ([**1**]^0), 2*H*-indazole ([**2**]^0), 1*H*-imidazole ([**3**]^0), and 1*H*-benzimidazole ([**4**]^0)) were synthesized as previously reported in the literature.[18]

$(H_2pz)[Os^{III}Cl_4(Hpz)_2]$ (H_2pz[1]). $NaBH_4$ (10.5 mg, 0.27 mmol) was added to a suspension of $[Os^{IV}Cl_4(Hpz)_2]$ ([**1**]^0) (118 mg, 0.25 mmol) in methanol (2 mL). The clear solution was stirred for 30 min and filtered. Then a solution of pyrazole (18 mg, 0.26 mmol) in 6 M HCl (0.5 mL) was added. The resulting solid was filtered off, washed with water and diethyl ether, and dried *in vacuo*. Single crystals of X-ray diffraction quality were collected directly from the mother liquor. Yield: 108 mg, 80%. Anal. Calcd for $C_9H_{13}Cl_4N_6Os$ (M = 537.28 g·mol^{-1}): C, 20.11; H, 2.44; N, 15.65. Found: C, 20.29; H, 2.42; N, 15.27%. Electrospray ionization mass spectrometry (ESI-MS) in MeOH (negative): *m*/*z* 467.9 $[Os^{III}Cl_4(Hpz)_2]^-$, 331.8 $[Os^{III}Cl_4]^-$; ESI-MS in MeOH (positive): *m*/*z* 432.9 $[OsCl_3(Hpz)_2]^+$. Mid-infrared (MIR), ν, cm^{-1}: 571, 663, 771, 903, 1046, 1113, 1166, 1264, 1346, 1399, 1473, 1511, 3121, and 3325. UV−vis (DMSO), λ_{max}, nm (ε, M^{-1} cm^{-1}): 256 (7823), 275 (5775), 299 (5792), 391 sh (225). ^{1}H NMR (D_2O, 500.10 MHz): δ −22.33 (br. s, 2H), −7.82 (br. s, 2H), −0.60 (br. s, 2H), 6.60 (s, 1H, Hpz), 7.96 (s, 2H, Hpz) ppm.

$(H_2ind)[Os^{III}Cl_4(Hind)_2]$ (H_2ind[2]). $NaBH_4$ (9.5 mg, 0.25 mmol) was added to a suspension of $[Os^{IV}Cl_4(Hind)_2]$ ([**2**]^0) (112 mg, 0.20

Chart 3. Starting Compounds and Final Products Studied in This Work[a]

Starting compounds

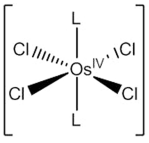

L	complex
Hpz	[**1**]^0
Hind	[**2**]^0
Him	[**3**]^0
Hbzim	[**4**]^0

Products investigated in this work (cation)

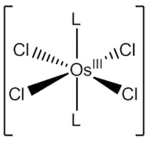

L	cation	complex
Hpz	H_2pz^+	H_2pz[**1**]
Hind	H_2ind^+	H_2ind[**2**]
Him	H_2im^+	H_2im[**3**]
Him	Ph_4P^+	Ph_4P[**3**]
Him	Bu_4N^+	Bu_4N[**3**]
Hbzim	H_2bzim^+	H_2bzim[**4**]
Hbzim	Ph_4P^+	Ph_4P[**4**]
Hbzim	Bu_4N^+	Bu_4N[**4**]

[a]Underlined complexes were investigated by X-ray crystallography.

dx.doi.org/10.1021/ic501710k | *Inorg. Chem.* 2014, 53, 11130−11139

mmol) in methanol (3 mL). The clear solution was stirred for 30 min and filtered. Then a solution of 1*H*-indazole (24 mg, 0.21 mmol) in 6 M HCl (1 mL) was added. The resulting solid was filtered off, washed with water and diethyl ether, and dried *in vacuo*. Single crystals of X-ray diffraction quality were collected from the mother liquor after slow evaporation of the solvent. Yield: 73 mg, 54%. Anal. Calcd for $C_{21}H_{19}Cl_4N_6Os\cdot MeOH$ (M = 719.50 g/mol): C, 36.72; H, 3.22; N, 11.68. Found: C, 36.40; H, 3.52; N, 12.03%. ESI-MS in MeOH (negative): *m*/*z* 567.9 $[Os^{III}Cl_4(Hind)_2]^-$, 332.5 $[Os^{III}Cl_4]^-$. ESI-MS in MeOH (positive): *m*/*z* 498.0 $[Os^{III}Cl_2(Hind)_2]^+$, 118.8 $[H_2ind]^+$. MIR, ν, cm^{-1}: 604, 672, 738, 809, 897, 1000, 1081, 1138, 1173, 1235, 1380, 1446, 1478, 1515, 1629, and 3330. UV−vis (DMSO), λ_{max}, nm (ε, M^{-1} cm^{-1}): 259 (17829), 368 (12516), 396 sh (9379), 615 (961). ^{1}H NMR (D_2O, 500.10 MHz): δ −11.02 (br. s, 2H), −0.23 (br. s, 2H), 1.39 (br. s, 2H), 7.12 (t, 1H, *J* = 7 Hz), 7.35 (t, 1H, *J* = 7 Hz), 7.55 (d, 1H, *J* = 8 Hz), 7.77 (d, 1H, *J* = 8 Hz), 8.08 (s, 1H), 13.00 (br. s, 1H) ppm.

$(H_2im)[Os^{III}Cl_4(Him)_2]$ (H_2im[3]). $NaBH_4$ (11 mg, 0.30 mmol) was added to a suspension of $[Os^{IV}Cl_4(Him)_2]$ ($[\mathbf{3}]^0$) (128 mg, 0.27 mmol) in methanol (3 mL). The clear solution was stirred for 30 min and filtered. Then a solution of imidazole (19 mg, 0.29 mmol) in 6 M HCl (1 mL) was added. The resulting solid was collected by filtration, washed with water, methanol, and diethyl ether and dried *in vacuo*. Yield: 135 mg, 90%. Anal. Calcd for $C_9H_{13}Cl_4N_6Os\cdot 0.5MeOH$ (M = 553.30 g/mol): C, 20.62; H, 2.73; N, 15.19. Found: C, 20.40; H, 2.45; N, 14.86%. ESI-MS in MeOH (negative): *m*/*z* 467.9 $[Os^{III}Cl_4(Him)_2]^-$, 332.2 $[Os^{III}Cl_4]^-$. ESI-MS in MeOH (positive): *m*/*z* 69.8 $[H_2im]^+$. MIR, ν, cm^{-1}: 616, 659, 748, 799, 1045, 1062, 1092, 1135, 1173, 1323, 1437, 1537, 1578, and 3135. UV−vis (DMSO), λ_{max}, nm (ε, M^{-1} cm^{-1}): 263 (7097), 293 (6316), 326 sh (1225), 378 (304). ^{1}H NMR (D_2O, 500.10 MHz): δ −19.43 (br. s, 2H), −14.07 (br. s, 2H), 2.85 (br. s, 2H), 7.41 (s, 2H), 8.59 (s, 1H) ppm.

$(Ph_4P)[Os^{III}Cl_4(Him)_2]$ (Ph_4P[3]). $NaBH_4$ (9.6 mg, 0.25 mmol) was added to a suspension of $[Os^{IV}Cl_4(Him)_2]$ ($[\mathbf{3}]^0$) (100 mg, 0.21 mmol) in methanol (4 mL), and the reaction mixture was stirred until the solution became clear. Ph_4PCl (84 mg, 0.22 mmol) was added, and the precipitated solid was collected by filtration, washed with methanol, and dried *in vacuo*. Yield: 97.7 mg, 56%. Anal. Calcd for $C_{30}H_{28}Cl_4N_4OsP\cdot H_2O$ (M = 825.60 g/mol): C, 43.64; H, 3.66; N, 6.79. Found: C, 43.52; H, 3.75; N, 6.61%. ESI-MS in MeOH (negative): *m*/*z* 467.9 $[Os^{III}Cl_4(Him)_2]^-$, 331.8 $[Os^{III}Cl_4]^-$. ESI-MS in MeOH (positive): *m*/*z* 339.1 $[Ph_4P]^+$. MIR, ν, cm^{-1}: 613, 663, 690, 754, 816, 996, 1059, 1109, 1325, 1440, 1484, and 3192. UV−vis (DMSO), λ_{max}, nm (ε, M^{-1} cm^{-1}): 270 (9234), 292 (5709), 331 sh (1011), 379 (299). ^{1}H NMR (DMSO-d_6, 500.10 MHz): δ −20.37 (br. s, 2H), −18.66 (br. s, 2H), 0.48 (br. s, 2H), 7.70−8.05 (m, 20H, Ph_4P) ppm.

$(nBu_4N)[Os^{III}Cl_4(Him)_2]$ (nBu_4N[3]). nBu_4NBH_4 (16 mg, 0.06 mmol) was added in two portions to a suspension of $[OsCl_4(Him)_2]$ ($[\mathbf{4}]^0$) (15 mg, 0.03 mmol) in methanol (2 mL). After 5 min the slightly turbid solution was filtered. The solution generated single crystals of X-ray diffraction quality upon standing at room temperature for 48 h.

$(H_2bzim)[Os^{III}Cl_4(Hbzim)_2]$ (H_2bzim[4]). $NaBH_4$ (8 mg, 0.21 mmol) was added to a suspension of $[Os^{IV}Cl_4(Hbzim)_2]$ ($[\mathbf{4}]^0$) (108 mg, 0.19 mmol) in methanol (3 mL). The clear solution was stirred for 30 min and filtered. Then a solution of benzimidazole (24 mg, 0.20 mmol) in 6 M HCl (1 mL) was added. The resulting solid was filtered off, washed with water, methanol, and diethyl ether, and dried *in vacuo*. Yield: 67 mg, 50%. Anal. Calcd for $C_{21}H_{19}Cl_4N_6Os\cdot 0.5MeOH$ (M = 703.48 g/mol): C, 36.70; H, 3.01; N, 11.95. Found: C, 36.74; H, 2.73; N, 11.60%. ESI-MS in MeOH (negative): *m*/*z* 568 $[Os^{III}Cl_4(Hbzim)_2]^-$, 332 $[Os^{III}Cl_4]^-$. ESI-MS in MeOH (positive): *m*/*z* 119 $[H_2bzim]^+$. MIR, ν, cm^{-1}: 591, 730, 1012, 1108, 1244, 1305, 1371, 1409, 1444, 1493, and 3295. UV−vis (DMSO), λ_{max}, nm (ε, M^{-1} cm^{-1}): 259 (14791), 299 (7130), 306 (7309), 331 sh (4582), 361 sh (2951), 423 (688), 498 (261). ^{1}H NMR (DMSO-d_6, 500.10 MHz): δ −17.85 (br. s, 2H), −5.23 (br. s, 2H), 2.02 (br. s, 2H), 4.22 (br. s, 2H), 4.39 (br. s, 2H), 5.74 (br. s, 2H), 7.55−7.60 (m, 2H), 7.83−7.88 (m, 2H), 9.40 (s, 1H), 14.57 (br. s, 1H) ppm.

$(Ph_4P)[Os^{III}Cl_4(Hbzim)_2]$ (Ph_4P[4]). $NaBH_4$ (8 mg, 0.21 mmol) was added to a suspension of $[Os^{IV}Cl_4(Hbzim)_2]$ ($[\mathbf{4}]^0$) (104 mg, 0.18 mmol) in water (4 mL). The clear solution was stirred for 30 min and filtered. Then tetraphenylphosphonium chloride (72 mg, 0.19 mmol) was added to the solution. The resulting solid was filtered off, washed with water and diethyl ether, and dried *in vacuo*. Yield: 113 mg, 67%. Anal. Calcd for $C_{38}H_{32}Cl_4N_4OsP\cdot H_2O$ (M = 925.72 g/mol): C, 49.30; H, 3.70; N, 6.05; O, 1.73. Found: C, 48.64; H, 3.52; N, 5.73; O, 1.94%. ESI-MS in MeOH (negative): *m*/*z* 567.9 $[Os^{III}Cl_4(Hbzim)_2]^-$, 331.8 $[Os^{III}Cl_4]^-$. ESI-MS in MeOH (positive): *m*/*z* 339.1 $[Ph_4P]^+$. MIR, ν, cm^{-1}: 614, 687, 720, 747, 828, 999, 1106, 1247, 1436, 1484, 1589, and 3197. UV−vis (DMSO), λ_{max}, nm (ε, M^{-1} cm^{-1}): 261 (13 794), 306 (6336), 361 sh (2496), 422 (608), 607 (525). ^{1}H NMR (DMSO-d_6, 500.10 MHz): δ −17.77 (br. s, 2H), −5.18 (br. s, 2H), 2.04 (br. s, 2H), 4.24 (br. s, 2H), 4.40 (br. s, 2H), 5.76 (br. s, 2H), 7.68−8.02 (m, 20H, Ph_4P) ppm.

$(nBu_4N)[Os^{III}Cl_4(Hbzim)_2]$ (nBu_4N[4]). nBu_4NBH_4 (26 mg, 0.10 mmol) was added in two portions to a suspension of $[OsCl_4(Hbzim)_2]$ ($[\mathbf{4}]^0$) (30 mg, 0.05 mmol) in water (3 mL). After 5 min the resulting pale green solid was filtered off, washed with water, methanol, and diethyl ether, and dried *in vacuo*. Yield: 32 mg, 77%. Anal. Calcd for $C_{30}H_{48}Cl_4N_5Os\cdot H_2O$ (M = 828.24 g/mol): C, 43.47; H, 6.08; N, 8.45; O, 1.91. Found: C, 43.25; H, 6.00; N, 8.23; O, 1.61%. ESI-MS in MeOH (negative): *m*/*z* 567.9 $[Os^{III}Cl_4(Hbzim)_2]^-$, 331.8 $[Os^{III}Cl_4]^-$. ESI-MS in MeOH (positive): *m*/*z* 242.3 $[Bu_4N]^+$. MIR, ν, cm^{-1}: 621, 748, 817, 884, 1007, 1151, 1252, 1309, 1438, 1486, 1623, 2964, and 3146. UV−vis (DMSO), λ_{max}, nm (ε, M^{-1} cm^{-1}): 260 (11 036), 306 (6299), 332 sh (3827), 360 sh (2413), 430 (438), 608 (455). ^{1}H NMR (DMSO-d_6, 500.10 MHz): δ −17.85 (br. s, 2H), −5.23 (br. s, 2H), 0.95 (t, 12H, *J* = 7 Hz), 1.34 (sext, 8H, *J* = 7 Hz), 1.55−1.65 (m, 8H), 2.02 (br. s, 2H), 3.14−3.22 (m, 8H), 4.22 (br. s, 2H), 4.39 (br. s, 2H), 5.74 (br. s, 2H) ppm.

Physical Measurements. Elemental analyses were performed by the Microanalytical Service of the Faculty of Chemistry of the University of Vienna and were carried out with a PerkinElmer 2400 CHN Elemental Analyzer. ^{1}H NMR (500.10 MHz) spectra were recorded on a Bruker Avance III instrument at 25 °C. ESI-MS measurements were carried out on a Bruker AmaZon SL ion trap spectrometer (Bruker Daltonics GmbH). The stability of the complexes in aqueous media at 25 °C was determined by UV−vis spectroscopy on a PerkinElmer Lambda 650 spectrometer in an optical cell of 1 cm path length in the wavelength range of 250−800 nm in combination with a PerkinElmer PTP-6 Peltier System.

Electrochemistry. Cyclic voltammograms (CVs) were measured in a three-electrode cell using a 2 mm diameter glassy carbon disk working electrode, a platinum auxiliary electrode, and a $Ag|Ag^+$ reference electrode containing 0.1 M $AgNO_3$. Measurements were performed at room temperature using an EG&G PARC potentiostat/galvanostat 273A. Deaeration of solutions was accomplished by purging a stream of argon through the solution for 5 min prior to each experiment. The potentials were measured in a freshly prepared solution of 0.1 M $(^nBu_4N)[BF_4]$ in DMSO using $[Fe(\eta^5\text{-}C_5H_5)_2]$ ($E_{1/2}$ = 0.68 V vs NHE)[29] as internal standard and are quoted relative to the normal hydrogen electrode (NHE).

The *in situ* spectroelectrochemical electron paramagnetic resonance (EPR)/UV−vis−NIR (NIR = near-infrared) experiments were carried out under argon atmosphere in a flat spectroelectrochemical cell, suitable for an optical transmission EPR resonator (ER 4104 OR-C 9609) of an EMX EPR spectrometer. The working electrode was a laminated Pt mesh with a small hole in the foil coincident with the light beam, which limited the active surface area of the electrode. A Pt-wire counter electrode and a Ag wire pseudoreference electrode were used. The optical EPR resonator cavity was connected to the diode-array UV−vis−NIR spectrophotometer Avantes Avaspec (Avantes, Netherlands) by optical fibers. A deuterium−halogen lamp DH 2000 (Sentronic, Germany) was used as a light source. UV−vis spectra were processed by the AvaSoft 7.7 software package. Both EPR and UV−vis−NIR spectrometers were synchronized together by trigger pulses

Table 1. Crystal Data and Details of Data Collection for H_2pz[1], H_2ind[2], and nBu$_4$N[3]

compound	H_2pz[**1**]	H_2ind[**2**]	nBu$_4$N[**3**]
empirical formula	$C_9H_{13}Cl_4N_6Os$	$C_{21}H_{19}Cl_4N_6Os$	$C_{22}H_{44}Cl_4N_5Os$
Fw	537.25	687.42	710.62
space group	$P2_1/c$	$P\bar{1}$	$Pbcn$
a, Å	7.4126(4)	9.4631(3)	14.7786(5)
b, Å	12.9016(6)	11.0678(4)	8.6629(3)
c, Å	16.1850(8)	13.6308(5)	22.4948(8)
α, deg		106.881(1)	
β, deg	94.636(2)	102.959(1)	
γ, deg		96.242(1)	
V, Å^3	1542.78(13)	1307.98(8)	2879.91(17)
Z	4	2	4
λ, Å	0.71073	0.71073	0.71073
ρ_{calcd}, g cm^{-3}	2.313	1.745	1.639
crystal size, mm	0.29 × 0.17 × 0.13	0.12 × 0.10 × 0.02	0.16 × 0.13 × 0.04
T, K	100(2)	100(2)	100(2)
μ, mm^{-1}	8.956	5.303	4.818
R_1[a]	0.0132	0.0172	0.0219
wR_2[b]	0.0306	0.0410	0.0481
GOF[c]	1.041	1.010	1.066

[a] $R_1 = \Sigma||F_0| - |F_c||/\Sigma|F_0|$. [b] $wR_2 = \{\Sigma[w(F_0^2 - F_c^2)^2]/\Sigma[w(F_0^2)^2]\}^{1/2}$. [c] GOF $= \{\Sigma[w(F_0^2 - F_c^2)^2]/(n - p)\}^{1/2}$, where n is the number of reflections and p is the total number of parameters refined.

received from the potentiostat. A Heka PG310USB (Lambrecht, Germany) potentiostat with a PotMaster 2.73 software package was used for the coulometric studies, and a Heka PG285 potentiostat (Lambrecht, Germany) with the same software equipment was used for the spectroelectrochemical studies. Sample solutions with approximate concentration of 0.5 mM, prepared with 0.2 M (^{n}Bu$_4$N)[PF$_6$] supporting electrolyte in DMSO, were purged with argon for 5 min prior to each experiment. A silver wire pseudoreference electrode was calibrated against an Fc/Fc$^+$ redox couple.

Crystallographic Structure Determination. X-ray diffraction measurements were performed on a Bruker D8 VENTURE CCD diffractometer. Single crystals were positioned at 35, 40, and 50 mm from the detector, and 731, 960, and 1735 frames were measured, each for 2.5, 30, and 10 s over 0.5, 0.25 and 0.5° scan width for (H_2pz)[Os^{III}Cl$_4$(Hpz)$_2$] (H_2pz[**1**]), (H_2ind)[Os^{III}Cl$_4$(Hind)$_2$] (H_2ind[**2**]), and ^{n}Bu$_4$N[Os^{III}Cl$_4$(Him)$_2$] (^{n}Bu$_4$N[**3**]), respectively. The data were processed using SAINT software.[30] Crystal data, data collection parameters, and structure refinement details are given in Table 1. The structures were solved by direct methods and refined by full-matrix least-squares techniques. Non-hydrogen atoms were refined with anisotropic displacement parameters. H atoms were inserted in calculated positions and refined with a riding model. The following computer programs and hardware were used: structure solution, *SHELXS-97*, and refinement, *SHELXL-97*;[31] molecular diagrams, and ORTEP.[32] The crystal structure of H_2ind[**2**] contained solvent, which could not be localized. Therefore, SQUEEZE option implemented in *PLATON*[33] was applied in the final refinement step.

Interaction with Small Biomolecules. The reactivity of complexes toward different amino acids (L-histidine, L-methionine, L-cysteine) was investigated. In particular, H_2pz[**1**] (2−3 mg/mL) and H_2bzim[**4**] (1 mg/mL) were dissolved in D_2O and treated with an equimolar amount of the respective amino acid, and the ^{1}H NMR spectra were recorded over 14−16 h at room temperature. Their DNA binding ability was examined by ^{1}H NMR spectroscopy by treatment with 2 equiv of 5′-dGMP solution in D_2O.

Cell Lines and Culture Conditions. Human cervical carcinoma (HeLa), human melanoma (FemX), human alveolar basal adenocarcinoma (A549), human colorectal adenocarcinoma (LS-174), human breast cancer (MDA-MB-453) cell lines, and normal human fetal lung fibroblast cell line (MRC-5) were maintained as monolayer culture in the Roswell Park Memorial Institute (RPMI) 1640 nutrient medium (Sigma Chemicals Co, USA). RPMI 1640 nutrient medium was prepared in sterile deionized water, supplemented with penicillin (192 U/mL), streptomycin (200 mg/mL), 4-(2-hydroxyethyl) piperazine-1-ethanesulfonic acid (HEPES) (25 mM), L-glutamine (3 mM), and 10% of heat-inactivated fetal calf serum (FCS) (pH 7.2). The cells were grown at 37 °C in 5% CO_2 in a humidified air atmosphere.

MTT Assay. Antiproliferative activity of tested osmium(III) complexes, KP1019, and cisplatin was determined using 3-(4,5-dymethylthiazol-yl)-2,5-diphenyltetrazolium bromide (MTT, Sigma-Aldrich) assay.[34] Cells were seeded into 96-well cell culture plates (Thermo Scientific Nunc) at a cell density of 4000 c/w (HeLa), 6000 c/w (A549), 4000 c/w (MDA-MD-453), 5000 c/w (FemX, MRC-5), and 7000 c/w (LS-174), in 100 μL of culture medium. After 24 h of growth, cells were exposed to the serial dilutions of the tested complexes, KP1019, and cisplatin. The osmium(III) complexes and KP1019 were dissolved in DMSO at a concentration of 30 mM as stock solution, and prior to use they were diluted with nutrient medium to the desired final concentrations (in range up to 300 μM). H_2ind[**2**] was dissolved in DMSO under an argon atmosphere to avoid direct contact of the substance with oxygen. Cisplatin (CDDP) stock solution was made in 0.9% NaCl at a concentration of 1.66 mM and afterward was diluted with nutrient medium to the desired final concentrations (in range up to 100 μM). Each concentration was tested in triplicate. Serial dilutions were made in culture medium so that the final concentration of DMSO per well was less than 1% (v/v) in all experiments. After incubation periods of 48 h, 20 μL of MTT solution (5 mg/mL in phosphate buffer, pH 7.2) was added to each well. Samples were incubated for 4 h at 37 °C, with 5% CO_2 in a humidified atmosphere. Formazan crystals were dissolved in 100 μL of 10% sodium dodecyl sulfate (SDS). Absorbances were recorded after 24 h, on an enzyme-linked immunosorbent assay (ELISA) reader (ThermoLabsystems Multiskan EX 200−240 V), at the wavelength of 570 nm. IC_{50} values (μM) were determined from the cell survival diagrams. The percentages of surviving cells relative to untreated controls were determined. The IC_{50} value, defined as the concentration of the compound causing 50% cell growth inhibition, was estimated from the dose−response curves.

RESULTS AND DISCUSSION

Synthesis and Characterization of the Complexes. While osmium analogues of NAMI-A have been documented in the literature,[19] the corresponding osmium(III) counterparts of KP1019 have not yet been reported. This is mainly because of

dx.doi.org/10.1021/ic501710k | Inorg. Chem. 2014, 53, 11130−11139

distinct differences in coordination chemistry of ruthenium and osmium with chlorido and azole ligands and a clear tendency to lower oxidation states for ruthenium compared to osmium upon sequential substitution of chlorido ligands by azole heterocycles in $[M^{IV}Cl_6]^{2-}$ (M = Ru, Os).

Starting from $(H_2azole)_2[Os^{IV}Cl_6]$ and by exploring the Anderson-type transformations, two families of osmium(IV) complexes, namely, $(H_2azole)[Os^{IV}Cl_5(Hazole)]$[20] and *trans*-$[Os^{IV}Cl_4(Hazole)_2]$,[18] were synthesized. The availability of compounds $[\mathbf{1}]^0$–$[\mathbf{4}]^0$ (Chart 3) has prompted us toward the final step to synthesize osmium(III) analogues of KP1019, namely, one-electron electrochemical or chemical reduction.

Dimethyl sulfoxide solutions of $[\mathbf{1}]^0$–$[\mathbf{4}]^0$ show intense charge-transfer absorptions in the visible region of optical spectra reaching extinction coefficients (ε) of over 10 000 M^{-1} cm^{-1} (Figure 1).[18] Of note is a strong blue shift of bands in the

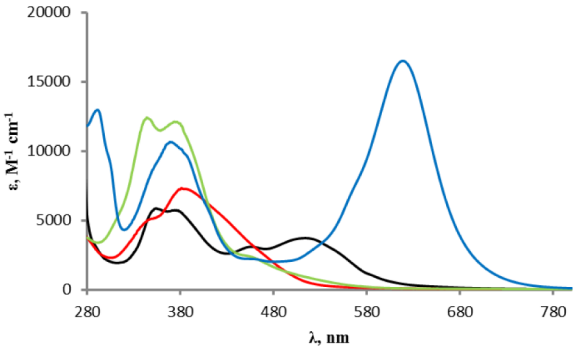

Figure 1. UV–vis spectra of the osmium(IV)-complexes $[\mathbf{1}]^0$ (red), $[\mathbf{2}]^0$ (blue), $[\mathbf{3}]^0$ (green), and $[\mathbf{4}]^0$ (black) adapted from ref 18.

visible region of the spectrum of $[\mathbf{2}]^0$ relative to Hpz, Him, and Hbzim complexes $[\mathbf{1}]^0$, $[\mathbf{3}]^0$, and $[\mathbf{4}]^0$, the origin of which is presumably due to a large variation of the dipole moment (of the order of several Debye) for an electron transfer from 2*H*-indazole to osmium.[11] Electrochemical reduction of complexes $[\mathbf{1}]^0$–$[\mathbf{4}]^0$ at 0.3 V led to a strong decrease of absorption in the visible region for $[\mathbf{1}]^-$, $[\mathbf{3}]^-$, $[\mathbf{4}]^-$ and that with maximum at about 628 nm for $[\mathbf{2}]^-$ and to an increase of bands in the UV-range of the spectrum to extinction coefficients exceeding 5000 M^{-1} cm^{-1} due to intraligand transitions of the azole heterocycles.

Strong absorption bands due to osmium(IV) regenerated by reoxidation of osmium(III) species by air oxygen provided further evidence for the reversible one-electron $Os^{IV/III}$ reduction.

More detailed investigation was performed with complex $[\mathbf{1}]^0$. A reversible cathodic reduction (the ratio of cathodic and anodic currents in the corresponding cyclic voltammogram is close to one) was observed even at a low scan rate (2 mV s^{-1}) in DMSO as shown in Figure 2a. Upon the *in situ* reduction at the first cathodic peak in DMSO the dominating absorption band at 386 nm decreased via an isosbestic point at 329 nm (Supporting Information, Figure S1). Simultaneously, a new band at 301 nm appeared. In addition, upon the voltammetric scan reversal a complete recovery of the $[\mathbf{1}]^0$ optical bands was observed indicating reversible electrochemical behavior and the high stability of cathodically generated $[\mathbf{1}]^-$ (Figure 2a).

To investigate the stability of $[\mathbf{1}]^-$, produced electrochemically at room temperature under argon, we performed an *ex situ* spectroelectrochemical experiment, where the corresponding

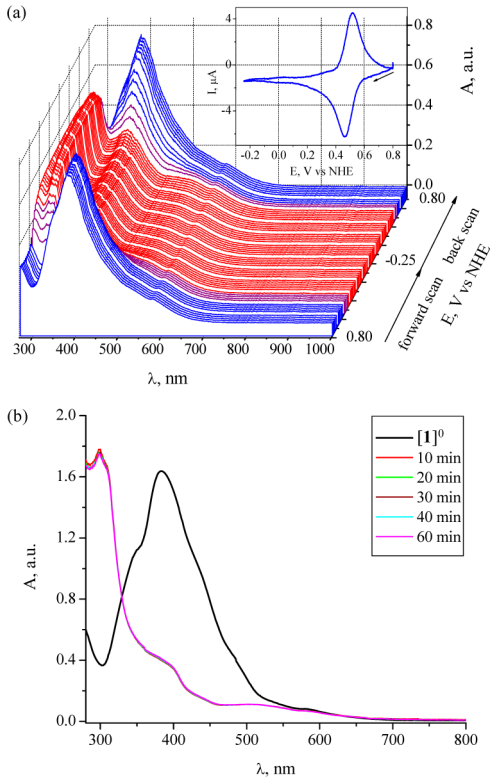

Figure 2. UV–vis spectroelectrochemistry of $[\mathbf{1}]^0$. (a) Electrochemical potential dependence of optical spectra with corresponding cyclic voltammogram (0.2 M $(n\mathrm{Bu_4N})[PF_6]$ in DMSO, scan rate 2 mV s^{-1}). (b) Optical spectrum of $[\mathbf{1}]^0$ in 0.2 M $(n\mathrm{Bu_4N})[PF_6]$/DMSO before (black line) and after bulk electrolysis at the first reduction peak (0.3 V vs NHE). The colored traces represent the optical spectra of the electrochemically generated species $[\mathbf{1}]^-$, measured at different time points after electrolysis.

sample $[\mathbf{1}]^0$ was electrolyzed in 0.2 M $(n\mathrm{Bu_4N})[PF_6]$ in DMSO in a special coulometric cell using a large platinum mesh working electrode at 0.3 V versus NHE. After a complete reduction the solution was inserted into the 1 cm UV cuvette, which was then immediately tightly closed to avoid contact with air oxygen, and UV–vis spectra were recorded at increasing time points. Figure 2b shows the absorption spectra of the initial $[\mathbf{1}]^0$ (black line) and one-electron reduced species $[\mathbf{1}]^-$ (colored lines) measured over time. Marginal changes in the spectrum of electrochemically generated species $[\mathbf{1}]^-$ (colored lines) confirmed the high stability of the product in DMSO. The stability data indicated that isolation of the osmium(III) species in the solid state after reduction of parent osmium(IV) complexes would be possible.

Therefore, we directed our efforts to the chemical reduction of complexes $[\mathbf{1}]^0$–$[\mathbf{4}]^0$ and isolation of the reduced species $[\mathbf{1}]^-$–$[\mathbf{4}]^-$ by addition of a certain salt as reductant and cation supplier. By reacting suspensions of $[\mathbf{3}]^0$ or $[\mathbf{4}]^0$ in water or methanol with a small excess tetrabutylammonium borohydride pale green solids of the composition $n\mathrm{Bu_4N}[\mathbf{3}]$ and $n\mathrm{Bu_4N}[\mathbf{4}]$ were isolated. Attempts to replace the tetrabutylammonium cation by the corresponding azolium ion via the sodium salts as reported for related osmium(IV) complexes[20] failed. Reduction of complexes $[\mathbf{3}]^0$ and $[\mathbf{4}]^0$ with $NaBH_4$ in methanol or water followed by addition of tetraphenylphosphonium chloride afforded complexes $PPh_4[\mathbf{3}]$ and $PPh_4[\mathbf{4}]$ in 56 and 67% yields, respectively. In addition, complexes $[\mathbf{1}]^-$–$[\mathbf{4}]^-$ were

dx.doi.org/10.1021/ic501710k | *Inorg. Chem.* 2014, 53, 11130–11139

prepared and isolated as azolium salts in 50 to 90% yields by reduction of $[\mathbf{1}]^0$–$[\mathbf{4}]^0$ in methanol with $NaBH_4$ and subsequent addition of the azole heterocycle in 6 M hydrochloric acid.

All complexes were characterized by ^{1}H NMR spectroscopy, and their spectra show signals of the azolium counterion as well as of the coordinated azole ligands. The signals of the coordinated azole heterocycles are broad and markedly upfield-shifted due to the paramagnetism of the osmium(III) center (d^5, $S = 1/2$).

UV–vis spectra of H_2pz[**1**], H_2ind[**2**], H_2im[**3**], and H_2bzim[**4**] in DMSO shown in Figure 3 are almost identical to those for $[\mathbf{1}]^-$–$[\mathbf{4}]^-$ generated upon the electrochemical reduction of $[\mathbf{1}]^0$–$[\mathbf{4}]^0$.

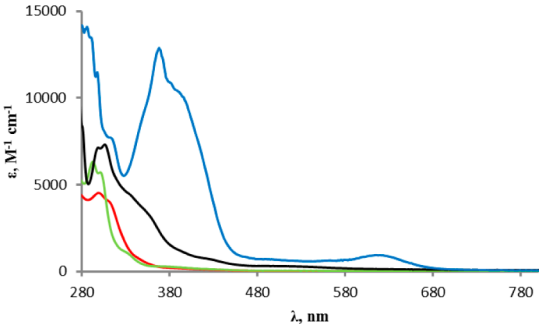

Figure 3. UV–vis spectra of the osmium(III) species $[\mathbf{1}]^-$ (red), $[\mathbf{2}]^-$ (blue), $[\mathbf{3}]^-$ (green), and $[\mathbf{4}]^-$ (black).

ESI mass spectra measured in both positive and negative ion modes are in agreement with the proposed composition for the eight isolated complexes. In particular, positive ion spectra for H_2ind[**2**] showed peaks with m/z 498.0 and 118.8 attributed to $[Os^{III}Cl_2(Hind)_2]^+$ and $[H_2ind]^+$, while those measured in the negative ion mode displayed signals at m/z 567.9 and 332.5, which are due to $[Os^{III}Cl_4(Hind)_2]^-$ and $[Os^{III}Cl_4]^-$, respectively. The presence of tetraphenylphosphonium and tetrabutylammonium cations in Ph_4P[**3**], Ph_4P[**4**] and nBu$_4$N-[**3**], nBu$_4$N[**4**] was confirmed by strong peaks with m/z 339.1 and 242.3, respectively, in their mass spectra.

X-ray Crystallography. The results of X-ray diffraction studies of complexes H_2pz[**1**], H_2ind[**2**], and nBu$_4$N[**3**] are shown in Figure 4. Selected bond lengths (Å) and bond angles (deg) are quoted in Table 2. Complex H_2pz[**1**] crystallized in

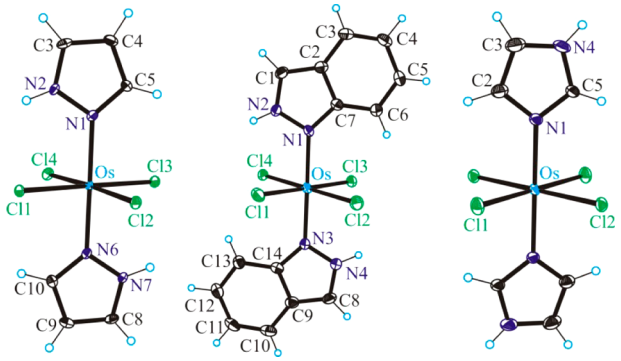

Figure 4. ORTEP view of complex anions $[Os^{III}Cl_4(Hpz)_2]^-$ (left), $[Os^{III}Cl_4(Hind)_2]^-$ (middle), and $[Os^{III}Cl_4(Him)_2]^-$ (right) in H_2pz[**1**], H_2ind[**2**], and nBu$_4$N[**3**]. Thermal ellipsoids are drawn at 50% probability level.

the monoclinic space group $P2_1/c$, while H_2ind[**2**] and nBu$_4$N-[**3**] crystallized in the triclinic centrosymmetric space group $P\bar{1}$ and orthorhombic space group *Pbcn*, respectively. There is one complex anion and one azolium counterion in the asymmetric unit of H_2pz[**1**] and H_2ind[**2**], while half of complex anion and half of counterion are in nBu$_4$N[**3**]. The osmium ion in nBu$_4$N[**3**] lies on a center of inversion, and the centrosymmetric complex anion is of point group symmetry C_i, while the nitrogen atom of the nBu$_4$N$^+$ resides on a 2-fold rotation axis (C_2). The osmium(III) ion in all three complex anions has an octahedral coordination geometry with four chlorido ligands in the equatorial plane and two azole heterocycles in axial positions.

The lengthening of the Os–N and Os–Cl bonds in $[\mathbf{1}]^-$, $[\mathbf{2}]^-$, and $[\mathbf{3}]^-$ compared to those in one-electron oxidized species $[\mathbf{1}]^0$, $[\mathbf{2}]^0$, and $[\mathbf{3}]^0$ is worth noting (Table 2). At the same time the Os–N and Os–Cl bonds in $[\mathbf{3}]^-$ are well-comparable with Ru–N and Ru–Cl at 2.078(5) and 2.360(2), 2.379(2) Å in $[Ru^{III}Cl_4(1H\text{-imidazole})_2]^-$,[35] and similar to those in $[Ru^{III}Cl_4(5\text{-nitro-}1H\text{-imidazole})_2]^-$.[36]

As in $[\mathbf{1}]^0$, $[\mathbf{2}]^0$, and $[\mathbf{3}]^0$,[18] both *trans*-azole ligands in $[\mathbf{1}]^-$, $[\mathbf{2}]^-$, and $[\mathbf{3}]^-$ are arranged parallel to each other in contrast to other related structures, for example, (Ph_4P)[*trans*-$Ru^{III}Cl_4(1H\text{-indazole})_2$], in which the azole ligands are significantly twisted.[37]

As in $[\mathbf{2}]^0$, the indazole ligand in $[\mathbf{2}]^-$ adopts a quinoid tautomeric form and binds to osmium(III) via nitrogen atom N1. This mode of coordination has been documented only for osmium(IV) so far,[11,18] and the reasons remain to be elucidated by theoretical studies of their electronic structure. The usual coordination mode of neutral indazole to a transition metal is via N2. Deprotonated indazole species act as a bridging ligand in polynuclear complexes[38,39] and in very rare cases as a monodentate indazolate ligand coordinated via N1 or N2.[40,41]

A varied number of hydrogen-bonding interactions is evident in the crystal structures of H_2pz[**1**], H_2ind[**2**], and nBu$_4$N[**3**], which are shown in Supporting Information, Figures S2–S5. The hydrogen-bonding parameters are summarized in Supporting Information, Tables S1–S3.

Stability in Aqueous Media and DMSO. The stability of metal complexes under physiological conditions is an important parameter in the development of potential metal-based drugs. The hydrolytic behavior of H_2pz[**1**] and H_2bzim[**4**] in aqueous media was monitored by ^{1}H NMR spectroscopy over 14 h, and no change in chemical shifts of the proton resonances was observed (Figures S6 and S7, see Supporting Information). However, a solid precipitated slowly from the aqueous solution of H_2bzim[**4**], which could be attributed to $[\mathbf{4}]^0$ by ESI-MS measurements. Note that aquation of KP1019 studied previously[42] resulted in formation of *mer,trans*-$[Ru^{III}Cl_3(Hind)_2(H_2O)]$, which was isolated and characterized by X-ray crystallography. The coordinated water molecule can be replaced by other nucleophilic ligands,[42] and, in particular, by nitric oxide.[43] It was suggested that the monoaqua species might play a role in the mechanism of action of KP1019.[42,43]

Some ruthenium-based potential anticancer drugs were shown recently[44] to undergo a fast replacement of monodentate ligands by DMSO solvent molecules upon dissolution. Therefore, the results of the *in vitro* MTT assays when using stock solutions of metal complexes in DMSO should be interpreted with care. The stability of complexes in DMSO is important for validation of the *in vitro* biological assays.[44] Complexes H_2pz[**1**], H_2ind[**2**], H_2im[**3**], and H_2bzim[**4**]

dx.doi.org/10.1021/ic501710k | Inorg. Chem. 2014, 53, 11130–11139

Table 2. Selected Bond Lengths (Å) and Angles (deg) in the Coordination Polyhedron of Osmium(III) in Complexes $[1]^-$, $[2]^-$, and $[3]^-$ and in One-Electron Oxidized Species $[1]^0$, $[2]^0$, and $[3]^0$ with Osmium in Oxidation State 4+ Reported Previously[18]

complex	$[1]^-$	$[2]^-$	$[3]^-$	$[1]^0$	$[2]^0$	$[3]^0$
Os–N	2.069(2) 2.059(2)	2.071(2) 2.061(2)	2.0752(17)	2.059(5)	2.050(5)	2.069(2)
Os–Cl	2.3872(6) 2.3868(6) 2.3834(6) 2.3411(6)	2.3760(6) 2.3666(7) 2.3992(6) 2.3883(6)	2.3780(5) 2.3735(5)	2.3301(14) 2.3326(14)	2.3439(16) 2.3395(15)	2.3381(6) 2.3139(6)

remain intact when dissolved in DMSO. Negative ion ESI mass spectra of these four complexes in DMSO solutions diluted with methanol 1:100 showed intense peaks attributed to $[Os^{III}Cl_4(Hazole)_2]^-$ and lack of ions that could hypothetically result from substitution of chlorido or azole ligands by DMSO. ^{1}H NMR spectra of H_2pz[**1**] in DMSO-d_6 remained unchanged over 16 h providing further evidence for the complex stability in solution (Figure 5). ^{1}H NMR measurements of H_2bzim[**4**] over 14 h gave the same results (Figure S8, see Supporting Information), although the color of the solution turned red during the investigated time frame, indicating minor reoxidation of $[4]^-$ to $[4]^0$ in the presence of air oxygen. Further UV–vis measurements over 168 h confirmed slow reoxidation of the benzannulated osmium(III) complex to osmium(IV) species (Supporting Information, Figure S9, lower) in contrast to H_2pz[**1**], which remained intact over the same time frame (Supporting Information, Figure S9, upper).

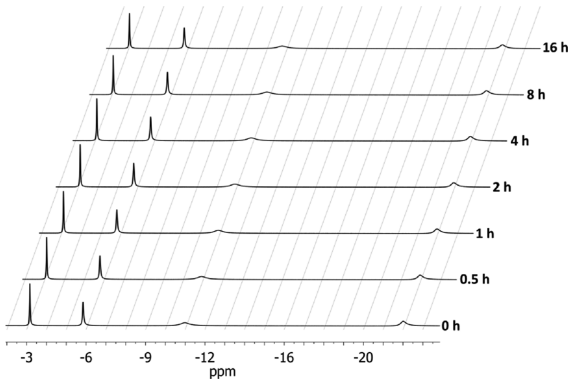

Figure 5. ^{1}H NMR spectra of H_2pz[**1**] in DMSO measured over 16 h.

Reactions with Small Biomolecules. Many drugs are administered intravenously, and once they have entered the bloodstream, amino acids and proteins are their first potential reaction partners. The reactions of potential anticancer agents with small biomolecules, such as amino acids, have been studied in solution by ^{1}H NMR spectroscopy[45−47] and occasionally by isolation and characterization of the resulting products in the solid state.[48] L-Histidine, L-methionine, and L-cysteine are known to form complexes with ruthenium and other transition metals[49,50] and play an important role in the mechanism of action of anticancer agents.[51−54] In addition, the reactivity of KP1019 toward DNA bases and thioethers has been reported.[55] Therefore, the interactions of complex H_2pz[**1**] with the three amino acids L-histidine, L-methionine, and L-cysteine and the DNA nucleotide 5′-dGMP were investigated by ^{1}H NMR spectroscopy in addition to the previously described aquation experiments.

Solutions of H_2pz[**1**] were treated with equimolar amounts of the respective amino acid, and the reactions were monitored by ^{1}H NMR spectroscopy for at least 14 h. H_2pz[**1**] remained intact in solution over the investigated time frame in the presence of L-histidine and L-cysteine as well as L-methionine (Figure 6). The hydrolytic stability of H_2pz[**1**] and lack of reactivity toward biomolecules are presumably responsible for its low antiproliferative activity in the investigated human cancer cell lines (vide infra). Since benzannulated complexes have shown appreciable antiproliferative activities in several human cancer cell lines (vide infra), similar measurements were conducted for H_2bzim[**4**]. However, there was no difference in reactivity of H_2bzim[**4**] compared to that of H_2pz[**1**] observed. As found during the investigations of the hydrolytic stability, a solid precipitated slowly from the H_2bzim[**4**] solutions with amino acids, which could be attributed to $[4]^0$ by ESI-MS measurements, and no amino acid adduct formation was seen.

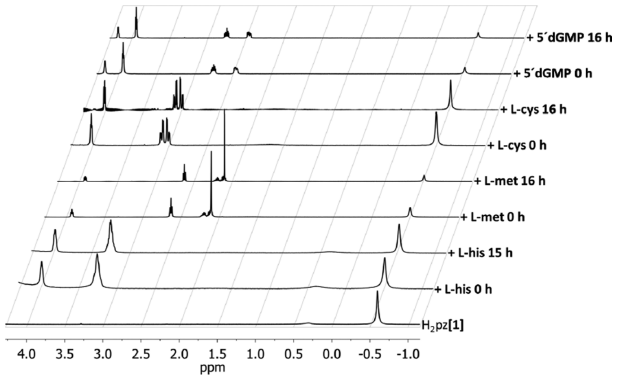

Figure 6. ^{1}H NMR spectra of reaction mixtures of H_2pz[**1**] with L-histidine, L-methionine, L-cysteine, and the DNA nucleotide 5′-dGMP in D_2O measured over 15–16 h.

Cyclic Voltammetry. The cyclic voltammograms of the complexes H_2pz[**1**], H_2ind[**2**], H_2im[**3**], and H_2bzim[**4**] in 0.1 M (nBu$_4$N)[BF$_4$]/DMSO at a glassy carbon working electrode with a scan rate of 0.2 V s^{-1} display a reversible one-electron oxidation wave attributed to the $Os^{III} \rightarrow Os^{IV}$ process with $E_{1/2}$ values ranging from 0.31 to 0.50 V versus NHE and an irreversible reduction wave attributed to the $Os^{III} \rightarrow Os^{II}$ process with E_p potential values between −1.16 and −1.53 V versus NHE (Figure 7, Table 3, and Supporting Information, Figures S6–S8). The obtained values are in good agreement with previously reported data for complexes $[1]^0$–$[4]^0$.[18] The $Os^{III} \rightarrow Os^{IV}$ waves are characterized by a peak-to-peak separation (ΔE_p) of 79–87 mV and an anodic peak current (i_{pa}) that is almost equal to the cathodic peak current (i_{pc}), as expected for electrochemically reversible processes. The reversible character of the redox process was further confirmed by a linear plot obtained for the peak current (i_p) versus square-root of scan rate ($\nu^{1/2}$).

The one-electron nature of the electron-transfer process was verified by comparing the peak current height with that of standard ferrocene/ferrocenium couple under identical experimental conditions. In our detailed spectroelectrochemical

dx.doi.org/10.1021/ic501710k | Inorg. Chem. 2014, 53, 11130−11139

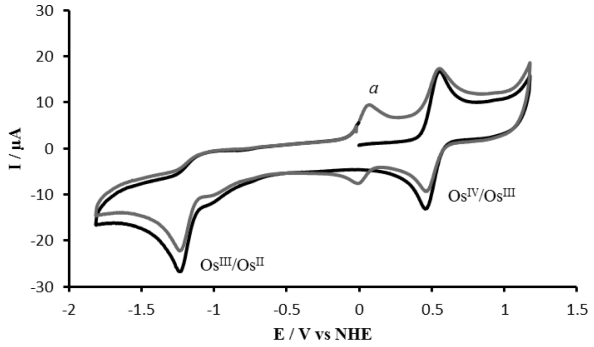

Figure 7. Cyclic voltammogram of H_2pz[**1**] in DMSO containing 0.10 M (^{n}Bu$_4$N)[BF$_4$] at a scan rate of 0.20 V s^{-1} using a glassy carbon working electrode; scan one is shown in black, scan two in gray.

study (vide supra), the controlled potential electrolysis performed at the first reduction peak for $[\mathbf{1}]^0$ showed the consumption of one electron per molecule (n = 0.95).

All investigated osmium(III) complexes appear to undergo solvolysis upon reduction due to cathodically induced metal dechlorination yielding the mono-DMSO species, as reported in the literature for related ruthenium complexes.[42] The appearance of the new species can be assigned to the oxidation peak *a* at −0.23 to 0.03 V (Figure 7, gray line, Table 3, and Supporting Information, Figures S10−S12).

The $Os^{III} \rightarrow Os^{II}$ redox potentials as well as those of the reductively induced solvolysis products have been calculated using the Lever's parametrization approach (eq 1);[56] [$S_M(Os^{III}/Os^{II})$ = 1.29;[57] $I_M(Os^{III}/Os^{II})$ = −0.39;[57] $E_L(Cl^-)$ = −0.24;[56] E_L(Hpz) = 0.20;[56] E_L(2*H*-ind) = 0.18;[11] E_L(Him) = 0.12;[56] E_L(Hbzim) = 0.10;[56] E_L(*S*-DMSO) = 0.57. The calculated values are quoted in Table 3 and are in good agreement with the experimental data.[58]]

$$E = S_M \cdot \sum E_L + I_M \qquad \text{(eq 1)}$$

MTT Assays. The antiproliferative activity of osmium(III)-complexes H_2pz[**1**], H_2ind[**2**], H_2im[**3**], H_2bzim[**4**], KP1019 and cisplatin was evaluated for 48 h of continuous drug action, using colorimetric MTT assay. The study was performed in five human neoplastic cell lines (HeLa, FemX, A549, MDA-MB-453, LS-174), and one human fetal lung fibroblast cell line (MRC-5), which was used as a noncancerous model for the *in vitro* toxicity evaluation. Results are summarized in Table 4 in terms of IC_{50} values for the 48 h incubation period. IC_{50} values are calculated as mean values obtained from two to three independent experiments and presented with their standard deviations (SDs).

Overall, the results indicate that osmium(III) complexes possess lower cytotoxic activity in all tested cell lines, compared to the lead compound KP1019. While the latter exhibits antiproliferative activity in all tumor cell lines, strong tumor-type selectivity was noted among active osmium(III) compounds. Complexes H_2pz[**1**] and H_2im[**3**] showed no cytotoxic activity in the tested range of concentrations (up to 300 μM). IC_{50} values for H_2ind[**2**] and H_2bzim[**4**] were obtained in the tested range of concentrations (up to 100 μM), both having the highest cytotoxic effect in human melanoma cells, FemX (20.4 ± 6.0 μM and 25.8 ± 5.5 μM, respectively). Only H_2ind[**2**] exhibited cytotoxic activity against human colorectal adenocarcinoma cells (LS-174), which could be a promising result, concerning decreased sensitivity of this tumor type to treatment. H_2ind[**2**] and H_2bzim[**4**] showed similar cytotoxic activity to cisplatin in normal fetal lung fibroblast cell line (MRC-5), expressing lower toxicity than KP1019, which might be an advantage for the investigated complexes, since the MRC-5 cell line was used as a noncancerous model for the *in vitro* toxicity evaluation.

Considering the cytotoxicity results, it is obvious that benzannulation (regarded here as a fusion of an aromatic ring to 1*H*-pyrazole or 1*H*-imidazole ring) causes a great difference in antitumor activity *in vitro* between the complexes with similar structures. In particular, H_2ind[**2**] is more cytotoxic than complex H_2pz[**1**], and H_2bzim[**4**] is more active than H_2im[**3**]. It implies that the investigated complexes might differently interact with DNA, in terms of forming different DNA adducts, or produce reactive oxygen species with different efficiency. Therefore, our next goal is investigating and revealing the mechanistic basis underlying their cytotoxicity profile. Moreover, since there are studies confirming that NAMI-A has significant antimetastatic potential besides its low cytotoxicity, complexes H_2pz[**1**] and H_2im[**3**], having related structures, should also be considered for further antimetastatic activity investigations.[59,60]

Previously reported data showed that *trans*-[$Os^{IV}Cl_4$(2H-indazole)$_2$] exhibit significant antiproliferative activity *in vitro*,[18] with the IC_{50} values in a concentration range comparable with that of the clinically studied ruthenium complex (H_2ind)-[$Ru^{III}Cl_4$(Hind)$_2$] (KP1019). Those results are also similar to the cytotoxicity profile of osmium(III) counterpart H_2ind[**2**] investigated herein, although the cell lines and incubation times in the present study are different.

CONCLUSIONS

The synthesis of osmium(III) analogues of the ruthenium(III) investigational drug KP1019 has been realized via electrochemical and chemical reduction of previously reported osmium(IV) complexes, *trans*-[$Os^{IV}Cl_4$(Hazole)$_2$]. Note, however, that the direct analogue of KP1019, namely, (H_2ind)-[$Os^{III}Cl_4$(1*H*-indazole)] has not been prepared yet. The reasons behind stabilization of 2*H*-indazole tautomeric form upon coordination to osmium(IV) and osmium(III) can presumably be established by ongoing *ab initio* studies on the electronic structure of *trans*-[$Os^{IV}Cl_4$(2H-indazole)$_2$], which will be reported in due course. While osmium(IV) complexes show strong absorptions in the visible region of optical spectra,

Table 3. Cyclic Voltammetric Data for H_2pz[1**], H_2ind[**2**], H_2im[**3**], and H_2bzim[**4**]**[a]

complex	E_p Os(III/II)	E_{calc} Os(III/II)	E_p *a*	E_{calc} *a*	$E_{1/2}$ Os(IV/III), (ΔE_p)
H_2pz[**1**]	−1.23	−1.11	0.03	−0.07	0.50 (87)
H_2ind[**2**]	−1.16	−1.16	−0.01	−0.12	0.42 (85)
H_2im[**3**]	−1.53	−1.32	−0.23	−0.27	0.31 (79)
H_2bzim[**4**]	−1.44	−1.37	−0.16	−0.33	0.37 (82)

[a]The potentials are quoted in V vs NHE.

dx.doi.org/10.1021/ic501710k | *Inorg. Chem.* 2014, 53, 11130−11139

Table 4. Results of MTT Assay Presented as IC_{50} (μM) Values Obtained after 48 h of Treatment

	IC_{50}[a] [μM] (mean ± SD)					
complex	HeLa	A549	FemX	MDA-MB-453	LS-174	MRC-5
H_2pz[**1**]	>300	>300	>300	>300	>300	>300
H_2ind[**2**]	83.04 ± 0.9	>100	20.4 ± 6.0	>100	70.3 ± 5.5	33.8 ± 0.2
H_2im[**3**]	>300	>300	>300	>300	>300	>300
H_2bzim[**4**]	56.6 ± 4.0	>100	25.8 ± 5.5	>100	>100	31.5 ± 3.0
KP1019	23.9 ± 3.0	24.3 ± 9.7	6.4 ± 2.8	40.8 ± 15.0	48.0 ± 10.8	13.1 ± 4.7
CDDP	7.8 ± 2.3	17.2 ± 0.7	10.8 ± 0.9	21.0 ± 5.7	22.4 ± 7.2	30.3 ± 3.0

[a]The sign > (in front of the maximum value of the concentration) indicates that IC_{50} value is not reached in the examined range of concentrations.

with extinction coefficients exceeding 10 000 M^{-1} cm^{-1} in some cases, the osmium(III) complexes are characterized by much lower intensity absorptions in the visible region of the optical spectra. Single-crystal X-ray diffraction studies of H_2pz[**1**], H_2ind[**2**], and nBu$_4$N[**3**] have confirmed their formulation. One-electron reduction resulted in appreciable expansion of the coordination sphere about osmium manifested in the lengthening of the Os−N and Os−Cl bonds by 0.005−0.016 and 0.04−0.05 Å, respectively. There was no change in coordination mode of indazole observed upon reduction of [**2**]^0 to [**2**]$^-$. The cytotoxicity profiles of the investigated complexes suggest that osmium(III) analogues of KP1019 appear particularly interesting for future investigations of their biological activity *in vitro* and for further clinical development.

■ ASSOCIATED CONTENT

Supporting Information

UV−vis spectroelectrochemistry of [**1**]^0 (Figure S1), hydrogen-bonding interactions in H_2pz[**1**], H_2ind[**2**], and nBu$_4$N[**3**] (Figures S2−S5), hydrogen-bonding parameters (Tables S1−S3), cyclic voltammograms of H_2ind[**2**] (Figure S6), H_2im[**3**] (Figure S7), and H_2bzim[**4**] (Figure S8), ^{1}H NMR spectra of H_2pz[**1**] in D_2O measured over 16 h (Figure S9), ^{1}H NMR spectra of H_2bzim[**4**] in DMSO-d_6 measured over 14 h (Figure S10) and in D_2O measured over 16 h (Figure S11), UV−vis measurements of H_2pz[**1**] and H_2bzim[**4**] in DMSO over 168 h (Figure S12), and crystallographic data in CIF format. This material is available free of charge via the Internet at http://pubs.acs.org.

■ AUTHOR INFORMATION

Corresponding Author

*E-mail: vladimir.arion@univie.ac.at.

Notes

The authors declare no competing financial interest.

■ ACKNOWLEDGMENTS

We thank A. Dobrov for ESI mass spectra measurements, A. Roller for collection of the X-ray data, and M. Malarek for reading the manuscript and helpful discussion. We are thankful to the Ministry of Science and Technology of Serbia for financial support from Grant No. III41026. P.R. thanks the Science and Technology Assistance Agency (Contract No. SK-AT-0027-12) and Slovak Grant Agency VEGA (Grant No. 1/0307/14) for financial support.

■ REFERENCES

(1) Clarke, M. J. *Coord. Chem. Rev.* **2003**, *236*, 209−233.

(2) Antonarakis, E. S.; Emadi, A. *Cancer Chemother. Pharmacol.* **2010**, *66*, 1−9.

(3) Scolaro, C.; Bergamo, A.; Brescacin, L.; Delfino, R.; Cocchietto, M.; Laurenczy, G.; Geldbach, T. J.; Sava, G.; Dyson, P. J. *J. Med. Chem.* **2005**, *48*, 4161−4171.

(4) Peacock, A. F. A.; Melchart, M.; Deeth, R. J.; Habtemariam, A.; Parsons, S.; Sadler, P. J. *Chem.—Eur. J.* **2007**, *13*, 2601−2613.

(5) (a) Therrien, B.; Süss-Fink, G.; Govindaswamy, P.; Renfrew, A. K.; Dyson, P. J. *Angew. Chem., Int. Ed.* **2008**, *47*, 3773−3776. (b) Govender, P.; Edafe, F.; Makhubela, B. C. E.; Dyson, P. J.; Therrien, B.; Smith, G. S. *Inorg. Chim. Acta* **2014**, *409*, 112−120. (c) Govender, P.; Sudding, L. C.; Clavel, C. M.; Dyson, P. J.; Therrien, B.; Smith, G. S. *Dalton Trans.* **2013**, *42*, 1267−1277. (d) Tamasi, G.; Carpini, A.; Valensin, D.; Messori, L.; Pratesi, A.; Scaletti, F.; Jakupec, M. A.; Keppler, B.; Cini, R. *Polyhedron* **2014**, *81*, 227−237.

(6) Van Rijt, S. H.; Peacock, A. F. A.; Johnstone, R. D. L.; Parsons, S.; Sadler, P. J. *Inorg. Chem.* **2009**, *48*, 1753−1762.

(7) Filak, L. K.; Mühlgassner, G.; Bacher, F.; Roller, A.; Galanski, M.; Jakupec, M. A.; Keppler, B. K.; Arion, V. B. *Organometallics* **2011**, *30*, 273−283.

(8) Ibao, A.-F.; Gras, M.; Therrien, B.; Süss-Fink, G.; Zava, O.; Dyson, P. J. *Eur. J. Inorg. Chem.* **2012**, *2012*, 1531−1535.

(9) (a) Ni, W.-X.; Man, W.-L.; Yiu, S.-M.; Ho, M.; Cheung, M. T.-W.; Ko, C.-C.; Che, C.-M.; Lam, Y.-W.; Lau, T.-C. *Chem. Sci.* **2012**, *3*, 1582−1588. (b) Cardoso, C. R.; Lima, M. U. S.; Cheleski, J.; Peterson, E. J.; Venâncio, T.; Farell, N. R.; Carlos, R. M. *J. Med. Chem.* **2014**, *57*, 4906−4915.

(10) Suntharalingam, K.; Johnstone, T. C.; Bruno, P. M.; Lin, W.; Hemann, M. T.; Lippard, S. J. *J. Am. Chem. Soc.* **2013**, *135*, 14060−14063.

(11) Büchel, G. E.; Stepanenko, I. N.; Hejl, M.; Jakupec, M. A.; Keppler, B. K.; Heffeter, P.; Berger, W.; Arion, V. B. *J. Inorg. Biochem.* **2012**, *113*, 47−54.

(12) Stepanenko, I. N.; Krokhin, A. A.; John, R. O.; Roller, A.; Arion, V. B.; Jakupec, M. A.; Keppler, B. K. *Inorg. Chem.* **2008**, *47*, 7338−7347.

(13) Galanski, M.; Arion, V.; Jakupec, M.; Keppler, B. *Curr. Pharm. Des.* **2003**, *9*, 2078−2089.

(14) Jakupec, M. A.; Galanski, M.; Arion, V. B.; Hartinger, C. G.; Keppler, B. K. *Dalton Trans.* **2008**, 183−194.

(15) Alessio, E.; Mestroni, G.; Bergamo, A.; Sava, G. *Curr. Top. Med. Chem.* **2004**, *4*, 1525−1535.

(16) Trondl, R.; Heffeter, P.; Kowol, C. R.; Jakupec, M. A.; Berger, W.; Keppler, B. K. *Chem. Sci.* **2014**, *5*, 2925−2932.

(17) Bergamo, A.; Gaiddon, C.; Schellens, J. H. M.; Beijnen, J. H.; Sava, G. *J. Inorg. Biochem.* **2012**, *106*, 90−99.

(18) Büchel, G. E.; Stepanenko, I. N.; Hejl, M.; Jakupec, M. A.; Keppler, B. K.; Arion, V. B. *Inorg. Chem.* **2011**, *50*, 7690−7697.

(19) Cebrián-Losantos, B.; Krokhin, A. A.; Stepanenko, I. N.; Eichinger, R.; Jakupec, M. A.; Arion, V. B.; Keppler, B. K. *Inorg. Chem.* **2007**, *46*, 5023−5033.

(20) Büchel, G. E.; Stepanenko, I. N.; Hejl, M.; Jakupec, M. A.; Arion, V. B.; Keppler, B. K. *Inorg. Chem.* **2009**, *48*, 10737−10747.

(21) Doadrio, A.; Craciunescu, D.; Ghirvu, C.; Nuno, J. C. *An. Quim.* **1977**, *73*, 1220−1223.

(22) Singh, P.; Sarkar, B.; Sieger, M.; Niemeyer, M.; Fiedler, J.; Záliš, S.; Kaim, W. *Inorg. Chem.* **2006**, *45*, 4602−4609.

(23) Tröndlin, F.; Werner, R.; Rüchardt, C. *Chem. Ber.* **1978**, *111*, 367−378.
(24) Schmidt, A.; Beutler, A.; Snovydovych, B. *Eur. J. Org. Chem.* **2008**, 4073−4095.
(25) Seela, F.; Bourgeois, W. *Helv. Chim. Acta* **1991**, *74*, 315−322.
(26) Kazimierczuk, Z.; Lönnberg, H.; Vilpo, J.; Pfleiderer, W. *Nucleosides Nucleotides* **1989**, *8*, 599−617.
(27) Mosti, L.; Menozzi, G.; Fossa, P.; Schenone, P.; Lampa, E.; Parrillo, C.; D'Amisco, M.; Rossi, F. *Farmaco* **1992**, *47*, 567−584.
(28) (a) Lipinski, C. A.; Lombardo, F.; Dominy, B. W.; Feeney, P. J. *Adv. Drug Delivery Rev.* **2001**, *46*, 3−26. (b) Li, Y.; De Kock, C.; Smith, P. J.; Chibale, K.; Smith, G. S. *Adv. Drug Deliv. Rev.* **2014**, *33*, 4345−4348.
(29) Barrette, W. C., Jr; Johnson, H. W., Jr; Sawyer, D. T. *Anal. Chem.* **1984**, *56*, 1890−1898.
(30) Pressprich, M. R.; Chambers, J. *SAINT + Integration Engine, Program for Crystal Structure Integration;* Bruker Analytical X-ray systems; Bruker Analytical Xray systems: Madison, WI, 2004.
(31) Sheldrick, G. M. *Acta Crystallogr., Sect. A* **2008**, *64*, 112−122.
(32) Farrugia, L. J. *J. Appl. Crystallogr.* **1997**, *30*, 565−565.
(33) Spek, A. L. *PLATON: A Multipurpose Crystallographic Tool;* Utrecht University: The Netherlands, 2006.
(34) Supino, R. *In Vitro Toxicity Testing Protocols* **1995**, 137−149.
(35) Anderson, C.; Beauchamp, A. L. *Inorg. Chem.* **1995**, *34*, 6065−6073.
(36) Anderson, C.; Beauchamp, A. *Inorg. Chim. Acta* **1995**, *233*, 33−41.
(37) Peti, W.; Pieper, T.; Sommer, M.; Keppler, B. K.; Giester, G. *Eur. J. Inorg. Chem.* **1999**, 1551−1555.
(38) Rendle, D. F.; Storr, A.; Trotter, J. *Can. J. Chem.* **1975**, *53*, 2930−2943.
(39) Cortes-Llamas, S. A.; Hernández-Pérez, J. M.; Hô, M.; Muñoz-Hernández, M.-Á. *Organometallics* **2006**, *25*, 588−595.
(40) Schuecker, R.; John, R. O.; Jakupec, M. A.; Arion, V. B.; Keppler, B. K. *Organometallics* **2008**, *27*, 6587−6595.
(41) Fackler, J. P.; Staples, R. J.; Raptis, R. G. *Z. Kristallogr.* **1997**, *212*, 157−158.
(42) Cebrián-Losantos, B.; Reisner, E.; Kowol, C. R.; Roller, A.; Shova, S.; Arion, V. B.; Keppler, B. K. *Inorg. Chem.* **2008**, *47*, 6513−6523.
(43) Bučinský, L.; Büchel, G. E.; Ponec, R.; Rapta, P.; Breza, M.; Kožišek, J.; Gall, M.; Biscupič, S.; Fronc, M.; Schiessl, K.; Cuzan, O.; Prodius, D.; Turta, C.; Shova, S.; Zając; Arion, V. B. *Eur. J. Inorg. Chem.* **2013**, 2505−2519.
(44) Patra, M.; Joshi, T.; Pierroz, V.; Ingram, K.; Kaiser, M.; Ferrari, S.; Spingler, B.; Keiser, J.; Gasser, G. *Chem.—Eur. J.* **2013**, *19*, 14768−14772.
(45) Wang, F.; Chen, H.; Parkinson, J. A.; del S. Murdoch, P.; Sadler, P. J. *Inorg. Chem.* **2002**, *41*, 4509−4523.
(46) Wang, F.; Bella, J.; Parkinson, J. A.; Sadler, P. J. *J. Biol. Inor. Chem.* **2005**, *10*, 147−155.
(47) Paul, L. E. H.; Therrien, B.; Furrer, J. *Inorg. Chem.* **2012**, *51*, 1057−1067.
(48) Rathgeb, A.; Böhm, A.; Novak, M. S.; Gavriluta, A.; Dömötör, O.; Tommasino, J. B.; Enyedy, É. A.; Shova, S.; Meier, S.; Jakupec, M. A.; Luneau, D.; Arion, V. B. *Inorg. Chem.* **2014**, *53*, 2718−2729.
(49) Sheldrick, W. S.; Exner, R. *J. Organomet. Chem.* **1990**, *386*, 375−387.
(50) Sheldrick, W. S.; Gleichmann, A. *J. Organomet. Chem.* **1994**, *470*, 183−187.
(51) Reedijk, J. *Proc. Natl. Acad. Sci. U. S. A.* **2003**, *100*, 3611−3616.
(52) Reedijk, J. *Chem. Rev.* **1999**, *99*, 2499−2510.
(53) Chen, Y.; Guo, Z. J.; Murdoch, P. D.; Zang, E. L.; Sadler, P. J. *J. Chem. Soc., Dalton Trans.* **1998**, 1503−1508.
(54) Wang, F.; Xu, J.; Habtemariam, A.; Bella, J.; Sadler, P. J. *J. Am. Chem. Soc.* **2005**, *127*, 17734−17743.
(55) Egger, A.; Arion, V. B.; Reisner, E.; Cebrián-Losantos, B.; Shova, S.; Thettenhahn, G.; Keppler, B. K. *Inorg. Chem.* **2005**, *44*, 122−132.
(56) Lever, A. B. P. *Inorg. Chem.* **1990**, *29*, 1271−1285.
(57) Stepanenko, I. N.; Büchel, G. E.; Keppler, B. K.; Arion, V. B. Osmium Complexes with Azole Heterocycles as Potential Antitumor Drugs. In *Encyclopedia of Metalloproteins;* Springer: Berlin, Heidelberg, 2013; pp 1596−1614.
(58) Da Silva, M. F. C. G.; Pombeiro, A. J. L.; Geremia, S.; Zangrando, E.; Calligaris, M.; Zinchenko, A. V.; Kukushkin, V. Y. *J. Chem. Soc., Dalton Trans.* **2000**, 1363−1371.
(59) Bergamo, A.; Gava, B.; Alessio, E.; Mestroni, G.; Serli, B.; Cocchietto, M.; Sava, G. *Int. J. Oncol.* **2002**, *21*, 1331−1338.
(60) Cocchietto, M.; Zorzet, S.; Sorc, A.; Sava, G. *Invest. New Drugs* **2003**, *21*, 55−62.